



HAL
open science

Leaching of Metals in Coastal Technosols Triggered by Saline Solutions and Labile Organic Matter Removal

Hussein Jaafar Kanbar, Edward Elias Srouji, Zeinab Zeidan, Sirina Chokr, Zeinab Matar

► **To cite this version:**

Hussein Jaafar Kanbar, Edward Elias Srouji, Zeinab Zeidan, Sirina Chokr, Zeinab Matar. Leaching of Metals in Coastal Technosols Triggered by Saline Solutions and Labile Organic Matter Removal. *Water, Air, and Soil Pollution*, 2018, 229 (5), pp.157. 10.1007/s11270-018-3808-z . hal-03914183

HAL Id: hal-03914183

<https://hal.science/hal-03914183>

Submitted on 28 Dec 2022

HAL is a multi-disciplinary open access archive for the deposit and dissemination of scientific research documents, whether they are published or not. The documents may come from teaching and research institutions in France or abroad, or from public or private research centers.

L'archive ouverte pluridisciplinaire **HAL**, est destinée au dépôt et à la diffusion de documents scientifiques de niveau recherche, publiés ou non, émanant des établissements d'enseignement et de recherche français ou étrangers, des laboratoires publics ou privés.

Leaching of metals in coastal technosols triggered by saline solutions and labile organic matter removal

Hussein Jaafar Kanbar ^{a, b, *}, Edward Elias Srouji ^a, Zeinab Zeidan ^a, Sirina Chokr ^a, Zeinab Matar ^{a, c, *}

^a Research and Analysis Platform for Environmental Sciences (PRASE), Doctoral School of Sciences and Technology (EDST); Faculty of Sciences; The Lebanese University, P.O. 5, Rafic Hariri Campus, Hadat, Lebanon.

^b Applied Plant Biotechnology Laboratory (APBL); Faculty of Sciences; The Lebanese University, Rafic Hariri Campus, Hadat, Lebanon.

^c Department of Earth and Life Sciences; Faculty of Sciences; The Lebanese University, Rafic Hariri Campus, Hadat, Lebanon.

* Corresponding authors: Hsen.kanbar@gmail.com, ORCID ID: 0000-0002-9505-9974, telephone number: +961 71219629; matarzeinab@gmail.com, telephone number: +961 76971133

Abstract

This study aims to understand the influence of salinity and labile organic matter removal on the fate and behavior of metals in coastal technosols. Two technosol cores were collected near the Lebanese shore. The cores were sectioned into layers; each layer was characterized for pH, salinity, electric conductivity, labile and total organic matter, grain size, and total and oxalate-extractable metals. Consequently, two saline solutions were used in desorption experiments to understand the role of ionic strength and labile organic matter on metal release. The results showed that the technosol layers were highly heterogeneous; most layers were enriched with Fe, Zn, Pb and Cu. The mineralogical investigations showed that the metals, notably Fe, were not present as crystalline minerals, rather big percentages of the metals were found in amorphous or poorly crystalline phases. Desorption experiment showed that Mg release was dependent on salinity and organic matter in both technosols, while Pb release was dependent on both factors only in one. Additionally, Zn and Cu were associated to organic matter, and their release was conditioned by the removal of labile organic matter; iron was primarily found as amorphous or poorly crystalline phases, and salinity had a major role in its release. The role of ionic strength and labile organic matter removal on the behavior of metals in technosols was demonstrated. Finally, understanding metal dynamics between the solid and liquid compartments in technosols, especially where salt deposition occurs, is important to reduce unwanted metal leaching to groundwater or seawater and transfer to biota.

Keywords: technosol, desorption, metals, oxalate-extractable, ionic strength, labile organic matter

Acknowledgement

This research was financed by the research grant programs of the Lebanese University (The funding source had no involvement in the study design, writing of the report and decision to submit the article for publication). We would like to thank Prof. Ahmad Kobaissi (Lebanese University, Applied Plant Biotechnology Laboratory “APBL”) for giving us access to the flame photometer. The research assistants of the Research and Analysis Platform for Environmental Sciences (PRASE), namely Ms. Sarah Haddad, Ms. Sahar Rihane, Ms. Manal Houhou-Hadada, Mr. Ali Berro and Ms. Zahraa Ataya, are acknowledged for their dedicated work in sample analyses. We also thank Mr. Hussein Nasser who helped during the sampling campaign, Dr. Rawaa Ammar for reviewing an earlier version of this manuscript and an anonymous reviewer for their constructive comments.

40 **1. Introduction**

41 Lands covered by technosols have been gaining interest worldwide. Technosols are soils whose properties
42 or pedogenesis is predominated by technical origin (IUSS Working Group WRB, 2006); they develop on materials
43 resulting from human activities. Technosols commonly occur in urbanized and industrial regions, contain many
44 artefacts that are usually absent in natural soils (e.g. pesticides, sludge, cinder, slag and other industrial materials),
45 and can be enriched with organic compounds and metals (Huot et al., 2014a, 2014b; IUSS Working Group WRB,
46 2006; Monserie et al., 2009). In the near future, more technosols are expected to form due to urbanization, growth
47 of industrial sectors and the increasing demand for energy and mineral resources (Santini and Fey, 2016;
48 Scalenghe and Ferraris, 2009). Even though some technosols are recognized as metal and contaminant holding
49 zones, there is still a lack of information about the environmental fate of metals and contaminants in technosols.
50 In the case of metals, the major parameters that influence their behavior and fate are the initial metal species,
51 physico-chemical parameters of the matrix (e.g. solid and liquid phases of the technosol), such as pH, redox
52 potential and ionic strength (salinity), cation exchange capacity (CEC), and mineral, organic and vegetal
53 composition (Adriano, 2001; Butler, 2009; Carrillo-González et al., 2006; Du Laing et al., 2009).

54 Although technosols might be enriched with metals, they can further accumulate metals from different
55 sources, such as atmospheric depositions and surface run-off. Metal sorption augments if the technosols contain
56 fine particles (clayey), and are rich in organic matter (OM) and amorphous or poorly crystalline minerals, such as
57 allophanes and Fe oxyhydroxides (e.g. Latrille et al., 2003; Lynch et al., 2014). Indeed, the high surface area of
58 such particles can form abundant binding sites for metals (Du Laing et al., 2009; Wang et al., 2018). Furthermore,
59 the labile fraction of the organic matter (i.e. labile organic matter “LOM”) is the part that can be easily decomposed
60 by soil organisms (days to a few years). As a result, metals might be released from LOM, leach to water
61 compartments (e.g. groundwater or sea water) and can cause harmful effects with time (Charriau et al., 2011;
62 Strosser, 2010). Allophane-like phases have been reported to be present in volcanic soils and in materials where
63 similar high-temperature conditions predominate, such as in the byproducts and waste materials originated from
64 coal combustion, iron mining and steel making (e.g. sludge and slag from blast furnaces) (Parfitt and Kimble,
65 1989). Allophanes are mainly present in clay fractions, are made from hydrous aluminosilicates, and have
66 amorphous or poorly crystalline features (Hiradate, 2005; Wada and Wada, 1977). Moreover, allophanes were
67 proven to be present or even develop in technosols near steelmaking facilities (Huot et al., 2014b; Uzarowicz and
68 Skiba, 2011). In allophane rich technosols, OM tends to accumulate since the binding of these two components
69 (i.e. allophanes and OM) resist organic matter degradation (Buurman et al., 2007). Consequently, the mobility of
70 metals that are bound to allophanes, organic matter, or allophane-OM complexes might be limited or suspended
71 until further alterations cause metal release. Stable sulfide (or sulphide) formation under anoxic conditions (e.g.
72 water saturated technosols) or the integration of metals into well crystalline structures upon mineral crystallization
73 or soil ageing also reduces metal desorption (Du Laing et al., 2009; Manceau et al., 2002).

74 The Lebanese shore, located in the eastern part of the Mediterranean Sea (Levantine Sea), has been
75 recognized for shipping and trading activities since the Bronze Age (Elmaleh et al., 2012). As a result,
76 contaminated and technical soils and sediments have been present since a long time in Lebanon as well as other
77 sites that were famous for trading. Currently, Lebanon contains a lot of industries, especially on the shore; several

78 sites were reported to have signatures of anthropogenic activities, mainly by industrial and agrochemical plants
79 (Ammar et al., 2016, 2015; Kanbar et al., 2014). Soils, including technosols, located near seas/oceans undergo
80 unique processes; a key parameter that influences metal mobility at those sites is salinity (or ionic strength). Indeed,
81 sea breeze is carried to land where salts deposit; consequently, the cations released from the salts compete with
82 metals for binding sites, which causes the exchange between salt cations and sorbed metals. This might cause
83 unwanted metal desorption or leaching to nearby water bodies. Moreover, ionic strength, along with OM, is a
84 common parameter influencing metal sorption and desorption (e.g. Schlegel et al., 1999; Shi et al., 2013, 2005).
85 Therefore, technosols that are enriched with metals possibly associated to amorphous or poorly crystalline
86 minerals (such as allophanes and Fe oxyhydroxides), OM or a complex of both depict peculiar behavior, especially
87 for sites where salts are continuously deposited by sea breeze. Hence, this study will provide insights to the
88 potential environmental fate of metals in shoreline technosols that are susceptible to salt deposition.

89 The present study aims to characterize the technosols in terms of physico-chemical parameters, chemical
90 and mineralogical composition, and to determine the dynamics of metals between the solid (particulate) and liquid
91 (leachate) compartments of the technosols. More precisely, the effect of LOM removal and salinity on metal
92 desorption in metal-rich technosols is addressed. Accordingly, the understanding of the dynamics and fate of
93 metals under those conditions can help to manage technosols, to implement precaution strategies and to maintain
94 sustainable land. As a result, metal spreading and risk of transfer to biota can be downgraded or even stopped.

95 **2. Materials and Methods**

96 **2.1. Sampling site**

97 The technosols were collected near the Lebanese shore (Selaata, North Lebanon), located on the eastern
98 side of the Mediterranean Sea (**Fig. 1**). The Lebanese coast is characterized by a mild Mediterranean climate with
99 a cold and rainy winter (November till March) with temperatures ranging between 3 and 18°C, and a dry and
100 warm summer (May till September) with temperatures ranging between 18 and 38°C. The mean annual
101 precipitation on the Lebanese coast is 950 – 1000 mm. Surface water flows on the carbonaceous bedrock while
102 groundwater flows through karstic carbonate rocks, mainly resulting in the dissolution of carbonates (Metni et al.,
103 2004; Shaban, 2014). Agrochemical plants, fertilizer industries, wastewater treatment plants, tile factories, and a
104 steelmaking plant are located on the Lebanese shore, mainly in the north region (Selaata and Batroun). Local
105 studies were carried out on Lebanese soils (master studies at the Lebanese University, Faculty of Sciences) that
106 used X-ray fluorescence (XRF). The soils near the steelmaking plant were rather heterogeneous in composition,
107 yet a big part contained artefacts (mainly scrap) and were shown to be enriched with Fe, Pb, Zn, Cd and other
108 metals (XRF findings). As a result, the soils were identified as technosols and were chosen as the sampling site.
109 The technosol covers approximately 3000 m² and is not vegetated. It is important to note that the facility is active
110 only during certain periods of the year, so waste disposal directly from the facility is not continuous. Waste
111 materials and byproducts collected from the electric arc furnaces are usually reused in the furnaces; however,
112 metal-enriched materials harm the inner lining of furnaces and are therefore dumped. Those technosols are
113 expected to have allophanes which originate from the electric arc furnaces. Furthermore, other waste materials
114 from local and international industries have also been dumped at that location since approximately 10 years; those
115 introduced materials contribute to the presence of organic matter in the technosols, especially since the area behind

116 the steelmaking facilities is not vegetated. The area will serve as a dock after the dumped materials form an
 117 elevated land.

118 2.2. Sample collection, description and treatment

119 Technosols were collected via a motorized core drill behind the steelmaking industry (Percussion hammer
 120 Cobra TT, Eijkelkamp); the corer is 110 cm long and has a 90 mm diameter. Two cores were collected, hereby
 121 referred as NS and FS (collected near the sea and far the sea, respectively, **Fig. 1**). Those sites were chosen due
 122 to their distinct visual features as well as their locations away from the shoreline; different amounts of salt
 123 deposition from the sea are expected for the two sites. The NS and FS cores were located approximately 10 and
 124 40 meters away from the sea (**Fig. 1**) and were 40 and 87 cm deep, respectively. The NS core could not go deeper
 125 than 40 cm due to the presence of stones and coarse waste materials. The cores were sectioned according to visual
 126 aspects of the technosol layers (color, grain size, and presence of pebbles, stones and waste materials). The NS
 127 core was sectioned into 9 layers (NS1 to NS9), and the FS core was sectioned into 14 layers (FS10 to FS23). Some
 128 of the main properties of the layers that were used to section the cores are summarized in Table 1. All the 23 layers
 129 were frozen and freeze-dried. The bulk density and porosity (as well as particle density and solid space) were
 130 calculated using the dried samples (according to Thien and Graveel, 2003). The samples were then stored under
 131 dry conditions for further analyses. An aliquot of each sample was ground using an acid cleaned agate mortar and
 132 pestle.

Table 1: Main properties of the NS and FS technosol layers.
 BD: bulk density

Core	Layer (cm)	Label	Color	Properties (content)	BD (g/cm ³)	Porosity (%)
NS	0-3	NS1	dark brown	iron dust and scrap	1.1	44
	3-6	NS2		iron dust	1.3	50
	6-10	NS3		iron dust, glass materials and scrap	1.4	55
	10-20	NS4		stone and plastic materials	1.2	50
	20-22	NS5		white grains, plastic materials and scrap	1.2	50
	22-26	NS6		plastic and paper wastes	1.4	47
	26-30	NS7	scrap and plastic materials	1.3	50	
	30-35	NS8	beige	scrap	1.3	44
	35-40	NS9		scrap	1.3	68
FS	0-4	FS10	dark brown	scrap	1.2	45
	4-8	FS11		scrap and white grains	1.2	50
	8-16	FS12	sandy brown	scrap	-	-
	16-19	FS13		sticky texture and scrap	-	-
	19-24	FS14		sticky texture and white grains	1.1	48
	24-32	FS15		sticky texture	1.0	50
	32-50	FS16			-	-
	50-55	FS17			1.0	50
	55-61	FS18	light brown		-	-
	61-65	FS19			-	-
	65-71	FS20		sticky texture and white grains	-	-
	71-76	FS21			-	-
	76-81	FS22			-	-
	81-87	FS23			1.0	62

133 2.3. Physico-chemical characterization

134 The physico-chemical parameters, namely pH, salinity, electric conductivity (EC), total dissolved solids
135 (TDS), soil organic matter (total and labile) and grain sizes, were determined for all NS technosol layers and for
136 6 FS technosol layers. A duplicate measurement was done for each sample using non-ground aliquots unless
137 indicated otherwise. The pH was measured in a 1:1 ratio of soil:distilled water slurry using a combined soil pH
138 electrode (MA920B/1 from Milwaukee) coupled to a digital pH meter (AD1000 from ADWA), as described by
139 Burt (2004). Salinity, EC and TDS were measured according to AFNOR (NF ISO 11265, 1994) using a LaMotte
140 pH/TDS/Salt portable meter (Tracer PockeTester). Soil LOM and total OM, the latter represented by loss on
141 ignition (LoI), were determined after calcinating the samples. Dried and ground samples were calcinated at 250°C
142 for four hours; the mass difference was used to calculate soil LOM. The same samples were then heated at 550°C
143 for four hours, and the mass difference was used to calculate total organic matter (Heiri et al., 2001; Loh et al.,
144 2016). The particle size distribution of the technosols was carried out using laser diffraction method (Partica Laser
145 Scattering Particle Size Distribution Analyzer LA-950V2, from Horiba) with a range from 10 nm to 3000 µm.

146 **2.4. Mineralogical and chemical composition**

147 Dried and finely ground technosol samples were used for mineralogical and chemical composition
148 investigations. The major crystalline minerals were determined by qualitative X-ray diffraction (XRD) using a D8
149 Bruker X-ray diffractometer (copper anticathode of wavelength $\lambda_{K\alpha} = 1.5418 \text{ \AA}$). The diffractograms were
150 collected in the 2θ range of 10° to 60° with a step size of 0.034° per second. Functional groups were determined
151 by Fourier transform infrared (FTIR-6300 from JASCO). All technosol layers were analyzed using XRD and
152 FTIR; however, only relevant diffractograms and spectra are included in this paper.

153 Semi-quantitative XRF readings were done on all the layers of the two technosol cores. A pre-calibrated
154 handheld XRF gun equipped with an Ag anode and a generator of 45 kV maximum power was used (Niton XL2
155 Analyzer from Thermo Scientific). Sixty-second readings were performed on samples prepared on 2 cm holding
156 disks. Due to the sensitivity of the XRF gun, and due to the metal enrichment in the samples, only Ca, Fe, Zn and
157 Pb were semi-quantified. For selected layers of the NS and FS technosol cores, acid digestion was done via aqua
158 regia, as described by Kanbar et al. (2014). Although aqua regia does not dissolve silicate minerals, it was proven
159 to be a reliable technique for the determination of total metal contents (e.g. Melaku et al., 2005; Sastre et al., 2002;
160 Taraškevičius et al., 2013). Sodium and K were quantified using model 420 dual-mode flame photometer (from
161 Sherwood). Magnesium, Ca, Fe, Pb, Zn and Cu were measured using atomic absorption spectroscopy (AAS
162 Rayleigh WFX-210) equipped with a WF-10A autosampler, and flame and graphite furnace modes. Manually
163 prepared standards were used for calibration and QA/QC procedures were implemented based on internal
164 standards to reduce random errors.

165 Selective dissolution of allophanes as well as amorphous and poorly crystalline Fe oxyhydroxides or
166 ferrihydrites was done by acid oxalate method under darkness (AOD), which is also known as Tamm's method
167 (Pansu and Gautheyrou, 2006). This method was used to determine the metal contents associated with the
168 aforementioned minerals, which will be termed oxalate-extractable metals. The chemical composition was
169 determined by a flame photometer (for Na and K) and AAS (for Mg, Fe, Pb, Zn and Cu).

170 **2.5. Desorption experiments of bulk and calcinated technosols using salt solutions**

171 Desorption experiments were conducted to understand the release of metals as a function of salinity and
172 LOM removal. Salinity plays a crucial role in metal release, especially in coastal technosols and soils, while LOM
173 loss or degradation has a role in metal release in relatively short periods. Desorption experiments were made on
174 bulk and 250°C calcinated samples (the calcination process was presented in section 2.3). It should be noted that
175 XRD and FTIR analyses were also performed on the calcinated samples. However, two salt concentrations were
176 used in the desorption experiments (due to the different salinities of the technosols). Solutions of 200 and 1300
177 mg/L salinities were prepared, indicating low (LS) and high (HS) salinities, respectively. The LS and HS solutions
178 represent 0.5 and 2.9 mM ionic strengths, respectively. Calcium nitrate ($\text{Ca}(\text{NO}_3)_2$) was used as an electrolyte
179 because it is a neutral salt, i.e. it does not interact with exchanging processes; $\text{Ca}(\text{NO}_3)_2$ is commonly used in
180 metal exchange experiments (e.g. Camargo et al., 2007; Shi et al., 2013, 2008). Briefly, four desorption
181 experiments were done for each sample (i.e. bulk-LS, bulk-HS, 250-LS and 250-HS). A mass of 0.8 g of ground
182 soil (bulk and calcinated “250”) was added to 50 ml extracting solution (LS and HS). The mixtures were left 24
183 hours to stand before the experiment began so that swelling clays would have swelled (Keiser et al., 2014); this
184 was done to mimic actual conditions in the field and to give more accurate results on the metals released. The
185 mixtures were then stirred for 6 hours, filtered over 0.45 μm (cellulose acetate), the filtrates were acidified with
186 two drops of concentrated HNO_3 and stored at 4°C for metal quantification. The metals Mg, Fe, Pb, Zn and Cu
187 were quantified by AAS, and Na and K were quantified by flame photometry (AFP100 flame photometer, from
188 Biotech Engineering Management Co. LTD). The metal concentrations (in mg/L) released from the technosols
189 were converted to contents (either mg/kg or percent); consequently, a comparison could be made between the
190 desorbed metals on one hand, and the total and oxalate-extractable metals on the other.

191 **3. Results and Discussion**

192 **3.1. Physico-chemical parameters of the technosols**

193 Both technosol cores (NS and FS), even though located only 30 meters apart, have variable characteristics.
194 All the samples showed pH values above neutral (**Fig. 2**), indicating calcareous nature, which is a characteristic
195 of most Lebanese soils (Abdel-Rahman and Nader, 2002). As for salinity, EC and TDS, the NS technosols
196 significantly depicted elevated values, which ranged between 1040-1920 mg/L, 1970-3510 $\mu\text{S}/\text{cm}$ (equivalent to
197 1.9-3.5 dS/m) and 1460-2680 mg/L, respectively. On the other hand, those parameters were much lower for FS
198 technosols (190-320mg/L, 374-615 $\mu\text{S}/\text{cm}$ and 260-440 mg/L for salinity, EC and TDS, respectively). The exact
199 values for each layer are compiled in Table A1 (Online Resource). Although the technosols are rather
200 heterogeneous in composition and contained waste materials (Table 1), the high values of salinity, EC and TDS
201 are thought to be related to the location near the seashore (caused by sea breeze). Indeed, the relatively high EC
202 values in NS technosols were comparable to other soils collected near seas (e.g. Wang et al., 2014; Yu et al.,
203 2014). The organic fractions of NS and FS generally lied in the same ranges. However, NS samples contained
204 higher OM, mainly observed by lower LOM and OM limits for FS technosols. Samples with high LOM are
205 expected to have available nutrients or metals for biota (such as K, Mg, Fe, Mg, Zn and Cu), meaning that metal
206 release/desorption is higher (Strosser, 2010). As clearly seen by the grain size deciles (D_{10} , D_{50} and D_{90}), FS
207 samples are finer in texture than NS ones; more than 50% of the FS samples are made from silt and clay (D_{50} is
208 inferior to 64 μm ; Table A1, Online Resource). Moreover, the D_{10} values of the FS technosols, unlike NS ones,

209 indicate the presence of clay particles ($< 2 \mu\text{m}$). Furthermore, most of the FS samples, especially the deep ones,
210 had a sticky nature (Table 1), which reflects higher clay contents than NS samples. Organic matter and grain size
211 generally denote higher CEC on one hand, and higher total and exchangeable metals on the other. Indeed, soils
212 that are made of fine grains and contain high organic matter are expected to be more enriched with metals than
213 coarse and OM-poor soils (e.g. Carrillo-González et al., 2006; Kanbar et al., 2014; Manceau et al., 2002).

214 **3.2. Semi-quantification of metals in the technosols using XRF and possible sources**

215 The XRF findings were used to do an inter and intra-comparison between the NS and FS technosol samples.
216 The trends of Ca, Fe, Pb and Zn semi-contents are shown in **Fig. 3**. Calcium contents were higher in the top 40
217 cm of the FS technosols when compared to the deeper layers; moreover, pH of the FS technosols followed a
218 similar trend (Table A1, Online Resource), suggesting the contribution of Ca minerals in the calcareous technosols.
219 Although Ca is ubiquitous in Lebanese soils due to the predominance of carbonaceous formation (Abdel-Rahman
220 and Nader, 2002), it is also the main component present in steelmaking slag, since limestone and dolomite are
221 used in blast and electric arc furnaces to remove impurities (Das et al., 2007, 2002). Interestingly, NS technosols
222 were greatly enriched with Fe, and showed a general increase in depth. Even though Fe is the main element of
223 interest in steelmaking, it may still be present in byproducts or wastes if it cannot be extracted from the materials
224 used in the furnace; i.e. if Fe occurs as non-extractable species. Similar to iron, Pb and Zn contents were also
225 higher in the NS technosols when compared to FS samples. As for FS technosols, Pb and Zn were relatively higher
226 in the surface 20 cm layers. Iron, Zn and Pb are commonly found in waste materials released from steelmaking
227 facilities (Das et al., 2007; Kanbar et al., 2017; Kretzschmar et al., 2012). This, however, does not indicate that
228 the materials are entirely made from steelmaking wastes. Moreover, the trends of the metals were different even
229 for the same technosol core (e.g. different trends for Fe and Pb). An exception is the general decreasing trends of
230 Pb and Zn from the surface towards 20 cm depth, and quasi-steady contents afterward in the FS technosols. The
231 variability of metal contents in the same technosol core, or between the two cores, indicates that multiple sources
232 have contributed to the technosol formation. Finally, and according to the XRF findings (**Fig. 3**), the physico-
233 chemical characteristic (Table A1, Online Resource) and general properties of the technosol layers (Table 1),
234 some layers were selected for further characterization (namely NS1, NS4, NS9, FS11, FS14 and FS17). Those
235 samples are marked by a star in **Fig. 3**.

236 **3.3. Bulk mineralogical composition and chemical structure**

237 The diffractograms were fitted to quartz and calcite to correct the horizontal displacement; quartz and
238 calcite were used for fitting due to their predominance in the technosols. X-ray diffraction patterns revealed that
239 the well crystalline minerals present in the samples are primary silicate minerals (quartz), carbonate minerals
240 (calcite and dolomite) and secondary weathered silicate minerals (phyllosilicates; as indicated by the diffraction
241 lines at 4.47 and 2.57 Å) (**Fig. 4**). The NS and FS technosols have pH values in the range of 7.6-8.1 (**Fig. 2**) and
242 are therefore expected to contain calcite (Thomas, 2006). Dolomite was clearly identified in FS11 and FS17
243 technosols by the 2.88 Å peak. As stated previously, the detected dolomite might be originated from the
244 steelmaking facilities, since it is used to remove impurities, or it might be naturally found in soils of carbonaceous
245 formations (Abdel-Rahman and Nader, 2002; Das et al., 2007). Phyllosilicates were detected in the FS technosols;
246 indeed, FS technosols showed a clayey character in terms of size (small grain size deciles in **Fig. 2**) and sticky

247 texture (Table 1). Crystalline iron minerals were also detected in the technosols. Hematite (Fe_2O_3) or pyrite (FeS_2)
248 ($\sim 2.7 \text{ \AA}$) and magnetite (Fe_3O_4 , 2.53 \AA) were slightly detected in the NS technosols; NS layers are richer in Fe
249 than FS layers (**Fig. 3**). The relatively small peak at 2.7 \AA of the NS technosols makes it difficult to distinguish
250 between hematite and pyrite (2.69 and 2.71 \AA , respectively), hence the peak is assigned to either hematite or pyrite
251 (H/P), or can even be both. Goethite ($\alpha\text{-FeOOH}$, 4.18 \AA) was detected in the FS technosols. It is worth mentioning
252 that the diffractograms of the calcinated samples did not reveal additional information that the initial/bulk samples
253 did.

254 The FTIR spectra for the bulk and calcinated samples are shown in **Fig. 5**. From a general view, the bulk
255 FS14 and FS17 technosols showed a prominent peak at 1640 cm^{-1} , indicating bending mode of water molecules
256 and/or alkene functional group (Maréchal, 2011; Parikh et al., 2014). Since the samples were freeze-dried, the
257 water molecules indicated in the spectra are trapped in the interplanar spaces of clays (Schuttlefield et al., 2007);
258 indeed, diffractograms showed that the FS14 and FS17 technosols contain phyllosilicates (**Fig. 4**). Also, there is
259 a contribution of alkene (C=C) to the same peak due to its persistence in the calcinated samples for all technosols.
260 Bands between 2960 and 2855 cm^{-1} indicate alkyl functional groups ($-\text{CH}_3$, $-\text{CH}_2$ and CH), which in turn reflect
261 OM (Ammar et al., 2016; Kanbar et al., 2014; Le Meur et al., 2016). Those peaks were clearly shown in the bulk
262 NS technosols, especially NS1, which is the richest in OM (Table A1, Online Resource). Other bands that also
263 indicate OM are $1800\text{-}1400 \text{ cm}^{-1}$ (aliphatic or aromatic compounds) and 915 , 785 and 695 cm^{-1} (aromatic C-H)
264 (Margenot et al., 2015). After calcination, the bands assigned to OM naturally disappear due to the rupture of
265 hydrocarbon bonds. Moreover, bands between $930\text{-}730 \text{ cm}^{-1}$ and 1425 cm^{-1} could indicate calcite (Legodi et al.,
266 2001). The band at 2515 cm^{-1} could refer to thiol (S-H) or O-H group of carboxylic acid (Ammar et al., 2016;
267 Parikh et al., 2014), both which disappeared after calcination. Bands at 1115 and 1025 cm^{-1} indicate OM
268 (carboxylic acid C-O) as well as Si-O-Si of allophanes or quartz (Bishop et al., 2013; Levard et al., 2012;
269 Schuttlefield et al., 2007). Those peaks decreased after calcination, which could demonstrate the presence of
270 allophanes or quartz, since the latter surely remains intact after thermal treatment. Additionally, the bands at 520
271 and 465 cm^{-1} might also indicate salt or Si-O-Al out-of-plane bending for allophanes (Bishop et al., 2013; Parikh
272 et al., 2014; Pérez et al., 2016), the former is expected due to the location near the sea. Furthermore, the bands
273 located between 1300 and 900 cm^{-1} could also indicate allophanes (Prado et al., 2007; Rennert et al., 2014), in
274 addition to the other functional groups indicated in **Fig. 5**. The presence of a band at 627 cm^{-1} of the calcinated
275 samples indicates Fe-O vibrations of hematite or asymmetrical stretch of Fe-O of goethite; such minerals might
276 crystallize from Fe oxyhydroxides after thermal treatment. Metals might be released from the Fe oxyhydroxides
277 upon the formation of hematite and goethite (Lynch et al., 2014). The OH-stretching motion of interlayer hydroxyl
278 groups in kaolinite are assigned by the bands between 3800 and 3500 cm^{-1} (Ammar et al., 2016; Le Meur et al.,
279 2016; Schuttlefield et al., 2007), which were more prominent in the clay (phyllosilicate) containing FS technosols
280 and NS1 (**Fig. 4**). Other O-H groups are assigned at 3435 , 3351 and 3300 cm^{-1} , indicating O-H stretching of
281 carboxylic acids. After calcination, those peaks became more prominent due to the disappearance of organic
282 matter contributing to peaks in that region. Additionally, a small peak was detected at 3750 cm^{-1} in the calcinated
283 technosols, which belongs to the vibrational stretching of structural hydroxyl groups (Parikh et al., 2014).

284 **3.4. Total and oxalate-extractable metal contents, and behavior upon desorption** 285 **experiments**

286 The total metal contents confirmed the semi-quantitative XRF measurements, as seen by the similar trends
287 for the metals (Zn, Pb and Fe) in the two technosol cores (**Fig. 3**, **Fig. 6** and **Fig. 7**). Moreover, some of the metals
288 that were not semi-quantified by XRF showed to be distinct between the two technosol cores, namely Na, K and
289 Mg (**Fig. 6**). It is worth mentioning that due to the heterogeneity of the technosols (in terms of origin and contents),
290 the particle size did not correlate with metal contents (total, oxalate-extractable or desorbed), as it might be the
291 case of other studies.

292 **3.4.1. Behavior of major elements: Na, K, Mg and Ca**

293 Sodium contents were higher in the technosols having higher salinity, EC and TDS (i.e. NS technosols)
294 and were majorly released after oxalate extraction and desorption experiments (**Fig. 6a**). Even though Na salts
295 (mainly NaCl) were not detected by XRD, the presence of such salts can be affirmed by the location of NS
296 technosol near the seashore. Therefore, a part of the released Na is thought to come from Na salt dissolution, while
297 another part might come from the exchange caused by the $\text{Ca}(\text{NO}_3)_2$ salt in the desorption experiment. The high
298 total and oxalate-extractable Na in the NS samples could be reflected by high Na desorption after extraction with
299 salt solutions (LS and HS). Indeed, there exists a positive correlation between total and oxalate-extractable Na on
300 one hand, and desorbed or dissolved Na after desorption on the other (Table A2, Online Resource). Nonetheless,
301 different salt concentrations (or ionic strengths) and thermal treatment did not show to have an impact on Na
302 release. This is shown by similar Na contents released from bulk and calcinated samples upon desorption with LS
303 and HS solutions (**Fig. 6a**); again, this indicates that a big part of the dissolved Na originates from the dissolution
304 of Na salts. Moreover, K has higher affinity to soil particles than Na (Lal, 2006) and can be present in lattices as
305 a non-exchangeable element (Hodges, 2010); therefore, K is not leached as prominently as Na (**Fig. 6b**). Ammar
306 et al. (2016) showed that mainly Na, and to a lesser degree K, was exchanged with Ca in soils. The possible
307 presence of allophanes in the technosols was previously demonstrated by the FTIR (**Fig. 5**); a part of the released
308 K could originate from allophanes or amorphous or poorly-crystalline Fe oxyhydroxides, as seen by the positive
309 correlations between oxalate-extractable K and K released after desorption (Table A2, Online Resource).
310 Nevertheless, the correlation cannot be considered significant due to the low numbers of samples. In most cases,
311 more K was released using higher ionic strength solution (HS); this indicates that K forms exchangeable outer
312 sphere complexes (ionically bound) in soil particles, possibly in interlayer spaces of phyllosilicates (Butler, 2009;
313 Manceau et al., 2002). As for Mg, it was highly present in NS1 and NS4 technosols, however, only a minor part
314 was oxalate-extractable (**Fig. 6c**). On the other hand, NS9, FS11 and FS14 had relatively higher oxalate-
315 extractable Mg, which might suggest higher Mg desorption; this, however, was not the case. Disregarding oxalate-
316 extractable Mg, only a small part of Mg was desorbed from the bulk samples. Yet, Mg was significantly released
317 from the calcinated samples, in which HS solution showed more Mg desorption; again, this might indicate
318 exchangeable Mg as outer sphere complexes in the technosols. Indeed, this suggests Ca exchange (from the salt
319 solutions) with ionically held Mg. Moreover, in solutions with high ionic strength, divalent cations (Mg^{2+} in our
320 case) are more prone to desorption than monovalent ones (Hinsinger, 2006). Magnesium desorption after
321 removing LOM indicates that Mg had been initially associated with OM. At this stage, Mg^{2+} is the most cation to
322 be related to exchange with Ca^{2+} ; this, however, is only true for the calcinated samples (as seen by the positive
323 correlation between 250-LS and 250-HS, Table A2, Online Resource). As indicated mainly by XRD (calcite and
324 dolomite) and to a lesser extent by FTIR (**Fig. 4** and **Fig. 5**), the samples are enriched with Ca, except for FS17,

325 which contained the lowest Ca contents (**Fig. 6d**). Since the desorption solutions contain Ca (i.e. $\text{Ca}(\text{NO}_3)_2$), Ca
326 desorption will not be discussed in the desorption experiments.

327 **3.4.2. Fe mineralogy, chemical composition and role in metal sorption**

328 The NS technosol samples are enriched with Fe (12, 20 and 24% for NS1, NS4 and NS9, respectively; **Fig.**
329 **7a**). Due to that enrichment, well-crystalline Fe bearing minerals were expected to be detected by XRD, which
330 was not the case. In Fe rich technosols, soils and sediments, iron is found as oxides (hematite, wuestite “FeO” and
331 magnetite), oxyhydroxides (goethite), and sulfides (pyrite) (e.g. Huot et al., 2014b; Kanbar et al., 2017;
332 Montargès-Pelletier et al., 2014, 2007; Uzarowicz and Skiba, 2011). It should be noted that the absence of main
333 crystalline Fe bearing minerals in the XRD patterns was the main reason why oxalate-extractable Fe was addressed.
334 The peaks of hematite, goethite and magnetite were slightly detected in the diffractograms of NS and FS
335 technosols (**Fig. 4**); the low peaks suggest that Fe is majorly present as amorphous or poorly crystalline
336 oxyhydroxides. Poorly crystalline and amorphous phases are more reactive than crystalline minerals (Fey and
337 LeRoux, 1977; Lynch et al., 2014; Wada and Greenland, 1970). A big part of Fe was oxalate-extractable in NS1,
338 NS4, NS9 and FS11 technosols (**Fig. 7a**). Even though Fe can be associated to allophanes (ferriallophanes), the
339 high oxalate-extractable Fe suggests that they might be found as amorphous or poorly crystalline oxyhydroxides
340 as well. Iron desorption seemed rather heterogenous for the different technosol layers. Indeed, Fe is a major and
341 reactive element present in soils, in which precipitation and dissolution processes are diverse. This makes the
342 determination of Fe species and behavior in the environment highly interesting. What could be noted is a positive
343 correlation with electrolyte concentration for the bulk NS1 and NS4 technosols, while it was a negative correlation
344 for the FS technosols. After calcination, however, the released Fe contents were lower in comparison to the bulk
345 samples. Calcination of Fe oxyhydroxides can modify the structural arrangement of the chemically bonded water
346 and the -OH groups to produce crystalline phases (Lynch et al., 2014; Pansu and Gautheyrou, 2006); at 250°C,
347 hematite and goethite start to form (Longa-Avello et al., 2017). Although it could not be detected by XRD (**Fig.**
348 **4**), hematite and/or goethite formed in the calcinated samples, as suggested by the protrusion of the Fe-O peak in
349 the FTIR spectra (627 cm^{-1} , **Fig. 5**). During precipitation, metals might be released from or integrated into the
350 newly formed minerals (Lynch et al., 2014). Moreover, Fe rich allophanes or amorphous Fe phases (oxides or
351 oxyhydroxides) were proven to selectively sorb metals, such as Zn, Cu and Pb, some of which were found as
352 sulfides (Carrillo-González et al., 2006; Kanbar et al., 2017; Manceau et al., 2002; Uzarowicz and Skiba, 2011),
353 which might support the formation of Zn and Pb containing sulfides (for example in pyrite detected in the NS
354 samples, **Fig. 4**).

355 **3.4.3. Contents and fate of Pb, Zn and Cu in the technosols**

356 The NS technosols contain elevated Pb, Cu and Zn contents ($\sim 1000\text{ mg/kg}$ (0.1%) of Pb and 15000-22000
357 mg/kg (1.5-2.2%) of Zn in NS technosols, and $\sim 3000\text{ mg/kg}$ of Cu in NS4 and NS9 technosols, **Fig. 7: b-d**). Were
358 those metals present as crystalline minerals, their contents might be below the detection limits of the XRD, which
359 explains why Pb, Zn and Cu bearing minerals were not detected in the diffractograms (**Fig. 4**). Depending on the
360 crystallinity and level of the order of minerals, metals should be in the range of 0.5-5% to be detected on XRD
361 (Luxton et al., 2013). Another reason explaining the absence of Pb, Zn and Cu rich minerals by XRD, which is
362 more applicable here, is that their bearing phases are poorly crystalline or amorphous, such as Fe oxyhydroxides
363 or allophanes. Indeed, great fractions of Zn and Cu, and to a lesser extent Pb, were found as oxalate-extractable

364 (**Fig. 7: b-d**); those metals were reported to be associated to amorphous, poorly crystalline and organic phases
365 (Carrillo-González et al., 2006; Han and Singer, 2007; Manceau et al., 2002, 1996; Shi et al., 2013). Due to the
366 enrichment of Fe oxyhydroxides and/or Fe rich allophanes, Zn, Pb and Cu are thought to be present in those
367 phases, as well as in organic fractions. Nonetheless, it is not known if those metal-rich phases were initially
368 introduced to the technosol or if they formed as a result of different reactions through time. On the second
369 possibility, Huot et al. (2014b) showed that Fe rich allophane-like minerals formed in soils containing wastes from
370 an iron industry, which was considered as an early transformation or diagenesis. Other studies showed that the
371 weathering of aluminosilicate glass (in coal ash and blast furnace slag for example) can lead to the formation of
372 allophanes (Zevenbergen et al., 1999), especially in calcareous soils and under humid conditions (Bleam, 2017;
373 Sauer and Burghardt, 2006). In this study, the initial materials dumped in the sampling site could not be studied,
374 yet the formation of metal-rich allophanes and oxyhydroxides is highly anticipated. The high contents of Fe (total
375 and oxalate-extractable) and oxalate-extractable metals further support the presence of metals in allophanes, as
376 well as amorphous or poorly crystalline Fe oxyhydroxides. Additionally, poorly crystalline Fe rich
377 aluminosilicates were proven to form in metal-rich sediments (from steelmaking industries) and were able to retain
378 metals, such as Zn and Pb (Kanbar et al., 2017).

379 Even though Pb is generally considered as an immobile element, some treatments might promote Pb
380 desorption. In the case of NS and FS technosols, calcination caused higher Pb release in comparison to bulk
381 samples (**Fig. 7b**). This suggests that a major part of Pb might be complexed to organic fractions (as discussed
382 previously). As for the bulk samples, higher electrolyte solution caused higher Pb release for NS and FS technosols,
383 making the Ca-Pb exchange concentration dependent. This implies that Pb might also be found as outer sphere
384 complexes (Butler, 2009; Manceau et al., 2002); higher electrolyte solutions can release metals that are held in
385 interplanar spaces. On the other hand, when electrolyte concentration has no observable effect, only a small part
386 might be present in interplanar spaces, such as the case of FS samples, where phyllosilicates were prominently
387 detected (**Fig. 4**). Interestingly, 55-88% of Zn was oxalate-extractable, which partially explain why crystalline Zn
388 minerals were not detected in the samples containing 1.5-2% Zn (**Fig. 7c**). Moreover, Zn was found to be present
389 in Fe oxyhydroxides and allophane-like aluminosilicates (Huot et al., 2014b; Kanbar et al., 2017; Manceau et al.,
390 2002). In general, calcination increased Zn release (**Fig. 7c**). Additionally, and similarly to Pb, higher Ca^{2+} in the
391 solution caused higher Zn release; ionic strength was proven to influence Zn release in metal-rich sediments
392 (Butler, 2009). Several studies have shown that metal release after calcination is limited due to the integration of
393 metals in the precipitating iron oxides (e.g. Kribi et al., 2012; Ndiba et al., 2008). However, this is not the case in
394 the NS and FS technosols, where mainly Pb and to a lesser extent Zn desorption increased after calcination.
395 Therefore, metal integration in the precipitating Fe oxides is absent or limited. Alternatively, from the relatively
396 high oxalate-extractable Zn and Pb contents, and high Zn and Pb contents desorbed after calcination, those metals
397 are expected to be held by iron oxyhydroxides, amorphous phases and organic matter (Carrillo-González et al.,
398 2006; Han and Singer, 2007). Copper, like Zn and Pb, was released in higher contents after calcination (**Fig. 7d**).
399 Studies have shown that organic matter, in addition to Fe oxyhydroxides (Lynch et al., 2014), is the main holding
400 phase for Cu (Eggleton and Thomas, 2004; Weng et al., 2002). Indeed, copper release from technosols was
401 reported to be significantly higher for elevated pH values, which might be linked to the dissolution of organic
402 phases (Yao et al., 2009). The general high contents of Cu, Zn and Pb released in HS desorption experiments
403 suggest that those metals are not, or only rarely, found in sulfide minerals. The release of those metals was shown

404 to be independent of salinity in desorption experiments unless they were found as sulfides (Atkinson et al., 2007).
405 Finally, a graphic representation of the fate of metals (Mg, Fe, K, Pb, Zn and Cu) caused by saline solutions and
406 LOM removal for the two technosol cores is shown in **Fig. 8**. The release of metals upon the aforementioned
407 conditions can give insights on risk assessment, prevention strategies and consequent management of technosols
408 located near shorelines.

409 **4. Conclusion**

410 Layers of technosols collected near a steelmaking facility on the Lebanese shore were characterized for
411 physico-chemical parameters, mineralogical composition, and chemical contents (total and oxalate-extractable)
412 and behavior. Salinity, EC, TDS and grain sizes were different for the two technosol layers, while pH, OM and
413 LOM were comparable. The main crystalline minerals present in the technosols were quartz and calcite, while
414 few samples included phyllosilicates and dolomite. Despite the enrichment of Fe in the NS technosols, only
415 insignificant peaks of crystalline Fe minerals were detected by XRD; Fe was majorly present as amorphous or
416 poorly crystalline oxyhydroxides. Moreover, FTIR spectra suggested that allophane minerals are present in the
417 NS and FS technosols. Indeed, the metal-rich technosols showed that high percentages of metals (Fe, Pb, Zn and
418 Cu) were oxalate-extractable (amorphous or poorly crystalline), and thus explain the limited identification of
419 crystalline minerals, mainly Fe minerals, in the diffractograms. Those metals are chemically available upon
420 changes in physico-chemical parameters. Furthermore, desorption experiments supported that idea. The metals
421 Mg, Fe, Pb, Zn and Cu were desorbed in higher contents after LOM removal for most technosol samples. Salinity
422 showed to mainly affect Mg and Zn desorption, and to a lesser extent Fe and Pb. In the case of some technosols,
423 there was no effect of salinity concentration on metal release once the LOM was removed. This study highlights
424 the fate of metals in technosols near shorelines. By the deposition of salts and after the removal of LOM with time,
425 quantities of metals will be desorbed from the technosols and leach to groundwater or seawater, which might
426 cause destructive changes to the biota. Therefore, precautions should be taken to reduce saline solution deposition
427 (from seawater or sea breeze) to the high metal-available technosols by creating barriers between the sea and the
428 technosols, or by installing geomembranes to inhibit the migration of metal-containing leachates.

429 **5. Conflict of Interest**

430 The authors declare that they have no conflict of interest.

- 432 Abdel-Rahman, A.-F.M., Nader, F.H., 2002. Characterization of the Lebanese Jurassic-Cretaceous carbonate
433 stratigraphic sequence: a geochemical approach. *Geol. J.* 37, 69–91. <https://doi.org/10.1002/gj.902>
- 434 Adriano, D.C., 2001. Biogeochemical Processes Regulating Metal Behavior, in: *Trace Elements in Terrestrial*
435 *Environments*. Springer Science, New York, pp. 29–59. https://doi.org/10.1007/978-0-387-21510-5_2
- 436 Ammar, R., Kanbar, H.J., Kazpard, V., Wazne, M., El Samrani, A.G., Amacha, N., Saad, Z., Chou, L., 2016. Role
437 of phosphogypsum and NPK amendments on the retention or leaching of metals in different soils. *J. Environ.*
438 *Manage.* 178, 20–29. <https://doi.org/10.1016/j.jenvman.2016.04.042>
- 439 Ammar, R., Kazpard, V., Wazne, M., El Samrani, A.G., Amacha, N., Saad, Z., Chou, L., 2015. Reservoir
440 sediments: a sink or source of chemicals at the surface water-groundwater interface. *Environ. Monit. Assess.*
441 187, 4791. <https://doi.org/10.1007/s10661-015-4791-0>
- 442 Atkinson, C.A., Jolley, D.F., Simpson, S.L., 2007. Effect of overlying water pH, dissolved oxygen, salinity and
443 sediment disturbances on metal release and sequestration from metal contaminated marine sediments.
444 *Chemosphere* 69, 1428–1437. <https://doi.org/10.1016/j.chemosphere.2007.04.068>
- 445 Bishop, J.L., Ethbrampe, E.B., Bish, D.L., Abidin, Z.L., Baker, L.L., Matsue, N., Henmi, T., 2013. Spectral and
446 hydration properties of allophane and imogolite. *Clays Clay Miner.* 61, 57–74.
- 447 Bleam, W., 2017. Surface Chemistry and Adsorption, in: *Soil and Environmental Chemistry*. Elsevier, pp. 385–
448 443. <https://doi.org/10.1016/B978-0-12-804178-9.00008-2>
- 449 Burt, R., 2004. Soil Survey Laboratory Methods Manual. Soil Survey Laboratory Investigations Report No. 42.
450 USDA-NRCS.
- 451 Butler, B.A., 2009. Effect of pH, ionic strength, dissolved organic carbon, time, and particle size on metals release
452 from mine drainage impacted streambed sediments. *Water Res.* 43, 1392–1402.
453 <https://doi.org/10.1016/j.watres.2008.12.009>
- 454 Buurman, P., Peterse, F., Almendros Martin, G., 2007. Soil organic matter chemistry in allophanic soils: a
455 pyrolysis-GC/MS study of a Costa Rican Andosol catena. *Eur. J. Soil Sci.* 58, 1330–1347.
456 <https://doi.org/10.1111/j.1365-2389.2007.00925.x>
- 457 Camargo, I.M.C., Hiromoto, G., Flues, M., 2007. Heavy metal partition in acid soils contaminated by coal power
458 plant. *J. Braz. Chem. Soc.* 18, 831–837. <https://doi.org/10.1590/S0103-50532007000400024>
- 459 Carrillo-González, R., Šimůnek, J., Sauvė, S., Adriano, D.C., 2006. Mechanisms and pathways of trace element
460 mobility in soils, in: *Advances in Agronomy*. pp. 111–78. [https://doi.org/10.1016/S0065-2113\(06\)91003-7](https://doi.org/10.1016/S0065-2113(06)91003-7)
- 461 Charriau, A., Lesven, L., Gao, Y., Leermakers, M., Baeyens, W., Ouddane, B., Billon, G., 2011. Trace metal
462 behaviour in riverine sediments: Role of organic matter and sulfides. *Appl. Geochemistry* 26, 80–90.
463 <https://doi.org/10.1016/j.apgeochem.2010.11.005>
- 464 Das, B., Prakash, S., Reddy, P.S.R., Biswal, S.K., Mohapatra, B.K., Misra, V.N., 2002. Effective utilization of
465 blast furnace flue dust of integrated steel plants. *Eur. J. Miner. Process. Environ. Prot.* 2, 61–68.
- 466 Das, B., Prakash, S., Reddy, P.S.R., Misra, V.N., 2007. An overview of utilization of slag and sludge from steel
467 industries. *Resour. Conserv. Recycl.* 50, 40–57. <https://doi.org/10.1016/j.resconrec.2006.05.008>
- 468 Du Laing, G., Rinklebe, J., Vandecasteele, B., Meers, E., Tack, F.M.G., 2009. Trace metal behaviour in estuarine
469 and riverine floodplain soils and sediments: A review. *Sci. Total Environ.* 407, 3972–3985.
470 <https://doi.org/10.1016/j.scitotenv.2008.07.025>
- 471 Eggleton, J., Thomas, K. V., 2004. A review of factors affecting the release and bioavailability of contaminants
472 during sediment disturbance events. *Environ. Int.* 30, 973–980. <https://doi.org/10.1016/j.envint.2004.03.001>
- 473 Elmaleh, A., Galy, A., Allard, T., Dairon, R., Day, J.A., Michel, F., Marriner, N., Morhange, C., Couffignal, F.,
474 2012. Anthropogenic accumulation of metals and metalloids in carbonate-rich sediments: Insights from the
475 ancient harbor setting of Tyre (Lebanon). *Geochim. Cosmochim. Acta* 82, 23–38.
476 <https://doi.org/10.1016/j.gca.2011.04.032>
- 477 Fey, M. V., LeRoux, J., 1977. Properties and quantitative estimation of poorly crystalline components in
478 sesquioxidic soil clays. *Clays Clay Min.* 25, 285–294.
- 479 Han, F.X., Singer, A., 2007. Selective sequential dissolution for trace elements in arid zone soils, in: Alloway,
480 B.J., Trevors, J.T. (Eds.), *Biogeochemistry of Trace Elements in Arid Environments*. Springer, Dordrecht,
481 pp. 107–130. https://doi.org/10.1007/978-1-4020-6024-3_4
- 482 Heiri, O., Lotter, A.F., Lemcke, G., 2001. Loss on ignition as a method for estimating organic and carbonate
483 content in sediments: reproducibility and comparability of results. *J. Paleolimnol.* 25, 101–110.
484 <https://doi.org/10.1023/A:1008119611481>
- 485 Hinsinger, P., 2006. Potassium, in: Lal, R. (Ed.), *Encyclopedia of Soil Science*. CRC Press, pp. 1354–1358.
486 <https://doi.org/10.1081/E-ESS-120001716>
- 487 Hiradate, S., 2005. Structural changes of allophane during purification procedures as determined by solid-state
488 ²⁷Al and ²⁹Si NMR. *Clays Clay Miner.* 53, 653–658. <https://doi.org/10.1346/CCMN.2005.0530611>

489 Hodges, S.C., 2010. Soil fertility basics. North Carolina State University.

490 Huot, H., Faure, P., Biache, C., Lorgeoux, C., Simonnot, M.-O., Morel, J.-L., 2014a. A Technosol as archives of
491 organic matter related to past industrial activities. *Sci. Total Environ.* 487, 389–398.
492 <https://doi.org/10.1016/j.scitotenv.2014.04.047>

493 Huot, H., Simonnot, M.-O., Watteau, F., Marion, P., Yvon, J., De Donato, P., Morel, J.-L., 2014b. Early
494 transformation and transfer processes in a Technosol developing on iron industry deposits. *Eur. J. Soil Sci.*
495 65, 470–484. <https://doi.org/10.1111/ejss.12106>

496 IUSS Working Group WRB, 2006. World reference base for soil resources 2006. *World Soil Resour. Reports* 103.

497 Kanbar, H.J., Hanna, N., El Samrani, A.G., Kobaissi, A.N., Harb, N., Kazpard, V., Amacha, N., 2014. Metal
498 binding in soil cores and sediments in the vicinity of a dammed agricultural and industrial watershed.
499 *Environ. Monit. Assess.* 186, 8793–806. <https://doi.org/10.1007/s10661-014-4044-7>

500 Kanbar, H.J., Montargès-Pelletier, E., Losson, B., Bihannic, I., Gley, R., Bauer, A., Villieras, F., Manceau, L., El
501 Samrani, A.G., Kazpard, V., Mansuy-Huault, L., 2017. Iron mineralogy as a fingerprint of former
502 steelmaking activities in river sediments. *Sci. Total Environ.* 599–600, 540–553.
503 <https://doi.org/10.1016/j.scitotenv.2017.04.156>

504 Keiser, L., Soreghan, G.S., Joo, Y.J., 2014. Effects of drying techniques on grain-size analyses of fine-grained
505 sediment. *J. Sediment. Res.* 84, 893–896. <https://doi.org/10.2110/jsr.2014.68>

506 Kretzschmar, R., Mansfeldt, T., Mandaliev, P.N., Barmettler, K., Marcus, M.A., Voegelin, A., 2012. Speciation
507 of Zn in blast furnace sludge from former sedimentation ponds using synchrotron X-ray diffraction,
508 fluorescence, and absorption spectroscopy. *Environ. Sci. Technol.* 46, 12381–12390.
509 <https://doi.org/10.1021/es302981v>

510 Kribi, S., Ramarosan, J., Nzihou, A., Sharrock, P., Depelseñaire, G., 2012. Laboratory scale study of an industrial
511 phosphate and thermal treatment for polluted dredged sediments. *Int. J. Sediment Res.* 27, 538–546.
512 [https://doi.org/10.1016/S1001-6279\(13\)60011-6](https://doi.org/10.1016/S1001-6279(13)60011-6)

513 Lal, R., 2006. *Encyclopedia of Soil Science*. CRC Press.

514 Latrille, C., Denaix, L., Lamy, I., 2003. Interaction of copper and zinc with allophane and organic matter in the B
515 horizon of an Andosol. *Eur. J. Soil Sci.* 54, 357–364. <https://doi.org/10.1046/j.1365-2389.2003.00530.x>

516 Le Meur, M., Montargès-Pelletier, E., Bauer, A., Gley, R., Migot, S., Barres, O., Delus, C., Villieras, F., 2016.
517 Characterization of suspended particulate matter in the Moselle River (Lorraine, France): evolution along
518 the course of the river and in different hydrologic regimes. *J. Soils Sediments* 16, 1625–1642.
519 <https://doi.org/10.1007/s11368-015-1335-8>

520 Legodi, M.A., De Waal, D., Potgieter, J.H., Potgieter, S.S., 2001. Rapid determination of CaCO₃ in mixtures
521 utilising FT-IR spectroscopy. *Miner. Eng.* 14, 1107–1111. [https://doi.org/10.1016/S0892-6875\(01\)00116-9](https://doi.org/10.1016/S0892-6875(01)00116-9)

522 Levard, C., Doelsch, E., Basile-Doelsch, I., Abidin, Z., Miche, H., Masion, A., Rose, J., Borschneck, D., Bottero,
523 J.-Y., 2012. Structure and distribution of allophanes, imogolite and proto-imogolite in volcanic soils.
524 *Geoderma* 183, 100–108.

525 Loh, P.S., Chen, C.-T.A., Anshari, G.Z., Lou, J.-Y., Wang, J.-T., Wang, S.-L., Wang, B.-J., 2016. Sedimentary
526 organic matter and phosphate along the Kapuas River (west Kalimantan, Indonesia). *J. Chem.* 2016, 1–9.
527 <https://doi.org/10.1155/2016/6874234>

528 Longa-Avello, L., Pereyra-Zerpa, C., Casal-Ramos, J.A., Delvasto, P., 2017. Study of the calcination process of
529 two limonitic iron ores between 250 °C and 950 °C. *Rev. Fac. Ing.* 26, 33–45.
530 <https://doi.org/10.19053/01211129.v26.n45.2017.6053>

531 Luxton, T.P., Miller, B.W., Scheckel, K.G., 2013. Zinc Speciation Studies in Soil, Sediment and Environmental
532 Samples, in: Bakirdere, S. (Ed.), *Speciation Studies in Soil, Sediment and Environmental Samples*. CRC
533 Press, Taylor & Francis Groups, New York, pp. 433–477. <https://doi.org/doi:10.1201/b15501-12>

534 Lynch, S., Batty, L., Byrne, P., 2014. Environmental risk of metal mining contaminated river bank sediment at
535 redox-transitional zones. *Minerals* 4, 52–73. <https://doi.org/10.3390/min4010052>

536 Manceau, A., Boisset, M.-C., Sarret, G., Hazemann, J.-L., Mench, M., Cambier, P., Prost, R., 1996. Direct
537 determination of lead speciation in contaminated soils by EXAFS spectroscopy. *Environ. Sci. Technol.* 30,
538 1540–1552. <https://doi.org/10.1021/es9505154>

539 Manceau, A., Marcus, M.A., Tamura, N., 2002. Quantitative speciation of heavy metals in soils and sediments by
540 synchrotron X-ray techniques. *Rev. Mineral. Geochemistry* 49, 341–428.
541 <https://doi.org/10.2138/gsrmg.49.1.341>

542 Maréchal, Y., 2011. The molecular structure of liquid water delivered by absorption spectroscopy in the whole IR
543 region completed with thermodynamics data. *J. Mol. Struct.* 1004, 146–155.
544 <https://doi.org/10.1016/j.molstruc.2011.07.054>

545 Margenot, A., Calderón, F., Bowles, T., Parikh, S., Jackson, L., 2015. Soil organic matter functional group
546 composition in relation to organic carbon, nitrogen, and phosphorus fractions in organically managed
547 tomato fields. *Soil Sci. Soc. Am. J.* 79, 772–782. <https://doi.org/10.2136/sssaj2015.02.0070>

548 Melaku, S., Dams, R., Moens, L., 2005. Determination of trace elements in agricultural soil samples by inductively

549 coupled plasma-mass spectrometry: Microwave acid digestion versus aqua regia extraction. *Anal. Chim.*
550 *Acta* 543, 117–123. <https://doi.org/10.1016/j.aca.2005.04.055>

551 Metni, M., El-Fadel, M., Sadek, S., Kayal, R., Lichaa El Khoury, D., 2004. Groundwater Resources in Lebanon:
552 A Vulnerability Assessment. *Int. J. Water Resour. Dev.* 20, 475–492.
553 <https://doi.org/10.1080/07900620412331319135>

554 Monserie, M.-F., Watteau, F., Villemin, G., Ouvrard, S., Morel, J.-L., 2009. Technosol genesis: identification of
555 organo-mineral associations in a young Technosol derived from coking plant waste materials. *J. Soils*
556 *Sediments* 9, 537–546. <https://doi.org/10.1007/s11368-009-0084-y>

557 Montargès-Pelletier, E., Duriez, C., Ghanbaja, J., Jeanneau, L., Falkenberg, G., Michot, L.J., 2014. Microscale
558 investigations of the fate of heavy metals associated to iron-bearing particles in a highly polluted stream.
559 *Environ. Sci. Pollut. Res.* 21, 2744–2760. <https://doi.org/10.1007/s11356-013-2192-x>

560 Montargès-Pelletier, E., Jeanneau, L., Faure, P., Bihannic, I., Barres, O., Lartiges, B.S., 2007. The junction of
561 Fensch and Moselle rivers, France; mineralogy and composition of river materials. *Environ. Geol.* 53, 85–
562 102. <https://doi.org/10.1007/s00254-006-0621-6>

563 Ndiba, P., Axe, L., Boonfueng, T., 2008. Heavy metal immobilization through phosphate and thermal treatment
564 of dredged sediments. *Environ. Sci. Technol.* 42, 920–926. <https://doi.org/10.1021/es072082y>

565 NF ISO 11265, 1994. Qualité du sol—détermination de la conductivité électrique spécifique.

566 Pansu, M., Gautheyrou, J., 2006. Mineralogical Separation by Selective Dissolution, in: *Handbook of Soil*
567 *Analysis*. Springer Berlin Heidelberg, Berlin, Heidelberg, pp. 167–219. [https://doi.org/10.1007/978-3-540-](https://doi.org/10.1007/978-3-540-31211-6_4)
568 [31211-6_4](https://doi.org/10.1007/978-3-540-31211-6_4)

569 Parfitt, R.L., Kimble, J.M., 1989. Conditions for formation of allophane in soils. *Soil Sci. Soc. Am. J.* 53, 971.
570 <https://doi.org/10.2136/sssaj1989.03615995005300030057x>

571 Parikh, S.J., Goyne, K.W., Margenot, A.J., Calderón, F.J., 2014. Soil Chemical Insights Provided Through
572 Vibrational Spectroscopy, in: *Advances in Agronomy*. pp. 1–148. [https://doi.org/10.1016/B978-0-12-](https://doi.org/10.1016/B978-0-12-800132-5.00001-8)
573 [800132-5.00001-8](https://doi.org/10.1016/B978-0-12-800132-5.00001-8)

574 Pérez, N.A., Bucio, L., Lima, E., Soto, E., Cedillo, C., 2016. Identification of allophane and other semi-crystalline
575 and amorphous phases on pre-Hispanic Mexican adobe earth bricks from Cholula, Mexico. *Microchem. J.*
576 126, 349–358. <https://doi.org/10.1016/J.MICROC.2015.12.033>

577 Prado, B., Duwig, C., Hidalgo, C., Gómez, D., Yee, H., Prat, C., Esteves, M., Etchevers, J.D., 2007.
578 Characterization, functioning and classification of two volcanic soil profiles under different land uses in
579 Central Mexico. *Geoderma* 139, 300–313.

580 Rennert, T., Eusterhues, K., Hiradate, S., Breitzke, H., Buntkowsky, G., Totsche, K.U., Mansfeldt, T., 2014.
581 Characterisation of Andosols from Laacher See tephra by wet-chemical and spectroscopic techniques (FTIR,
582 27 Al-, 29 Si-NMR). *Chem. Geol.* 363, 13–21.

583 Santini, T.C., Fey, M. V., 2016. Assessment of Technosol formation and in situ remediation in capped alkaline
584 tailings. *CATENA* 136, 17–29. <https://doi.org/10.1016/j.catena.2015.08.006>

585 Sastre, J., Sahuquillo, A., Vidal, M., Rauret, G., 2002. Determination of Cd, Cu, Pb and Zn in environmental
586 samples: microwave-assisted total digestion versus aqua regia and nitric acid extraction. *Anal. Chim. Acta*
587 462, 59–72. [https://doi.org/10.1016/S0003-2670\(02\)00307-0](https://doi.org/10.1016/S0003-2670(02)00307-0)

588 Sauer, D., Burghardt, W., 2006. The occurrence and distribution of various forms of silica and zeolites in soils
589 developed from wastes of iron production. *CATENA* 65, 247–257.
590 <https://doi.org/10.1016/j.catena.2005.11.017>

591 Scalenghe, R., Ferraris, S., 2009. The first forty years of a technosol. *Pedosphere* 19, 40–52.
592 [https://doi.org/10.1016/S1002-0160\(08\)60082-X](https://doi.org/10.1016/S1002-0160(08)60082-X)

593 Schlegel, M.L., Charlet, L., Manceau, A., 1999. Sorption of metal ions on clay minerals. II. Mechanism of Co
594 sorption on hectorite at high and low ionic strength and impact on the sorbent stability. *J. Colloid Interface*
595 *Sci.* 220, 392–405. <https://doi.org/10.1006/jcis.1999.6538>

596 Schuttlefield, J.D., Cox, D., Grassian, V.H., 2007. An investigation of water uptake on clays minerals using ATR-
597 FTIR spectroscopy coupled with quartz crystal microbalance measurements. *J. Geophys. Res.* 112, D21303.
598 <https://doi.org/10.1029/2007JD008973>

599 Shaban, A., 2014. Physical and anthropogenic challenges of water resources in Lebanon. *J. Sci. Res. Reports* 3,
600 479–500.

601 Shi, Z., Di Toro, D.M., Allen, H.E., Ponizovsky, A.A., 2005. Modeling kinetics of Cu and Zn release from soils.
602 *Environ. Sci. Technol.* 39, 4562–4568. <https://doi.org/10.1021/es048554f>

603 Shi, Z., Di Toro, D.M., Allen, H.E., Sparks, D.L., 2013. A general model for kinetics of heavy metal adsorption
604 and desorption on soils. *Environ. Sci. Technol.* 47, 3761–7. <https://doi.org/10.1021/es304524p>

605 Shi, Z., Di Toro, D.M., Allen, H.E., Sparks, D.L., 2008. A WHAM - Based kinetics model for Zn adsorption and
606 desorption to soils. *Environ. Sci. Technol.* 42, 5630–5636. <https://doi.org/10.1021/es800454y>

607 Strosser, E., 2010. Methods for determination of labile soil organic matter: An overview. *J. Agrobiol.* 27, 49–60.
608 <https://doi.org/10.2478/s10146-009-0008-x>

609 Taraškevičius, R., Zinkutė, R., Stakėnienė, R., Radavičius, M., 2013. Case study of the relationship between Aqua
610 Regia and real total contents of harmful trace elements in some European soils. *J. Chem.* 2013, 1–15.
611 <https://doi.org/10.1155/2013/678140>

612 Thien, S.J., Graveel, J.G., 2003. *Laboratory Manual for Soil Science: Agricultural and Environmental Principles*,
613 8th ed. McGraw-Hill Publishing Company, Boston, MA.

614 Thomas, G.W., 2006. pH, in: Lal, R. (Ed.), *Encyclopedia of Soil Science*. CRC Press, pp. 1270–1274.

615 Uzarowicz, Ł., Skiba, S., 2011. Technogenic soils developed on mine spoils containing iron sulphides: Mineral
616 transformations as an indicator of pedogenesis. *Geoderma* 163, 95–108.
617 <https://doi.org/10.1016/j.geoderma.2011.04.008>

618 Wada, K., Greenland, D.J., 1970. Selective dissolution and differential infrared spectroscopy for characterization
619 of amorphous constituents in soil clays. *Clay Miner.* 8, 241–254.

620 Wada, S.-I., Wada, K., 1977. Density and structure of allophane. *Clay Miner.* 12, 289–298.

621 Wang, J.C., Hill, S.P., Dilbeck, T., Ogunsolu, O.O., Banerjee, T., Hanson, K., 2018. Multimolecular assemblies
622 on high surface area metal oxides and their role in interfacial energy and electron transfer. *Chem. Soc. Rev.*
623 <https://doi.org/10.1039/C7CS00565B>

624 Wang, Z., Zhao, G., Gao, M., Chang, C., Jia, J., Li, J., 2014. Characteristics and spatial variability of saline-
625 alkaline soil degradation in the typical Yellow River Delta area of Kenli County, China. *J. Environ. Prot.*
626 (Irvine, Calif.) 5, 1053–1063. <https://doi.org/10.4236/jep.2014.512104>

627 Weng, L., Temminghoff, E.J.M., Lofts, S., Tipping, E., Van Riemsdijk, W.H., 2002. Complexation with dissolved
628 organic matter and solubility control of heavy metals in a sandy soil. *Environ. Sci. Technol.* 36, 4804–4810.
629 <https://doi.org/10.1021/es0200084>

630 Yao, F.X., Macías, F., Virgel, S., Blanco, F., Jiang, X., Camps Arbestain, M., 2009. Chemical changes in heavy
631 metals in the leachates from Technosols. *Chemosphere* 77, 29–35.
632 <https://doi.org/10.1016/j.chemosphere.2009.06.012>

633 Yu, J., Li, Y., Han, G., Zhou, D., Fu, Y., Guan, B., Wang, G., Ning, K., Wu, H., Wang, J., 2014. The spatial
634 distribution characteristics of soil salinity in coastal zone of the Yellow River Delta. *Environ. Earth Sci.* 72,
635 589–599. <https://doi.org/10.1007/s12665-013-2980-0>

636 Zevenbergen, C., Bradley, J.P., van Reeuwijk, L.P., Shyam, A.K., Hjelmar, O., Comans, R.N.J., 1999. Clay
637 formation and metal fixation during weathering of coal fly ash. *Environ. Sci. Technol.* 33, 3405–3409.
638 <https://doi.org/10.1021/es9900151>

639

640

Figures

641

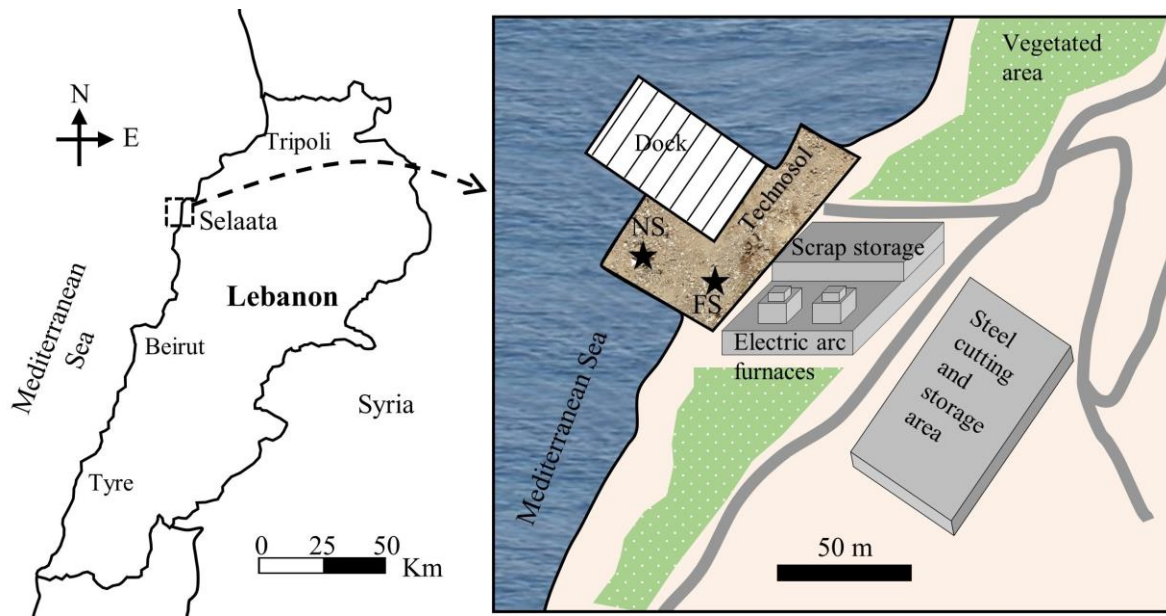


Fig. 1 Map of Lebanon (left) and the sampling sites at Selaata near the steelmaking facilities (right). The stars indicate the sites where the NS (near sea) and FS (far sea) technosol cores were collected

642

643

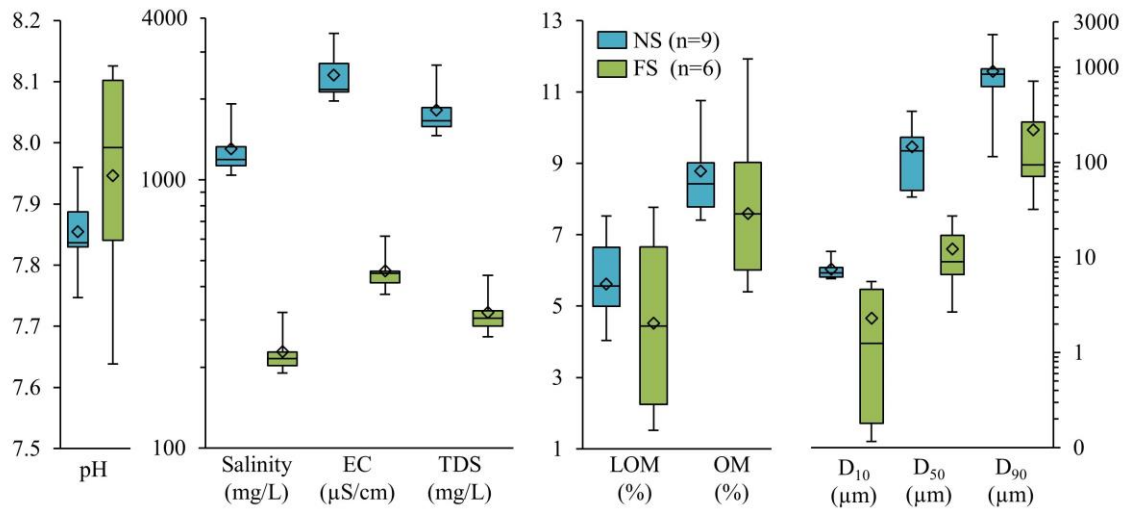


Fig. 2 Boxplots of pH, salinity, EC, TDS, LOM, OM, D₁₀, D₅₀ and D₉₀ values for the sets of NS and FS technosols.

White and gray plots refer to NS and FS samples, respectively. The lower and upper boundaries of the boxes refer to the 1st (Q25) and 3rd (Q75) quartiles, respectively. The horizontal lines in the boxes refer to the medians. The whiskers indicate the minimum and maximum values. The diamond shapes represent the averages

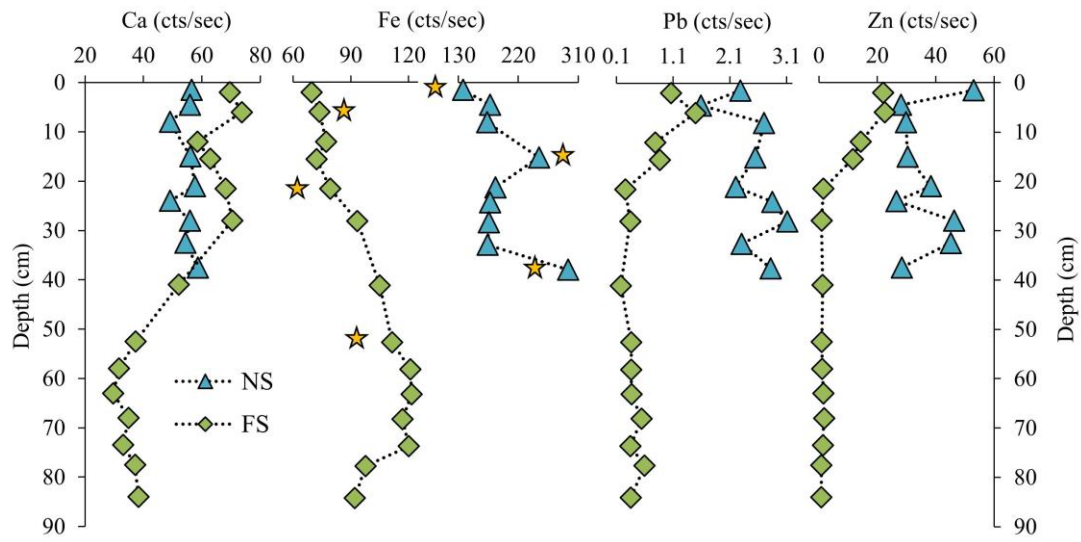


Fig. 3 Semi-quantitative metal contents (Ca, Fe, Pb and Zn, in counts/second) for the NS and FS technosols. Star symbols mark the samples that are presented hereafter

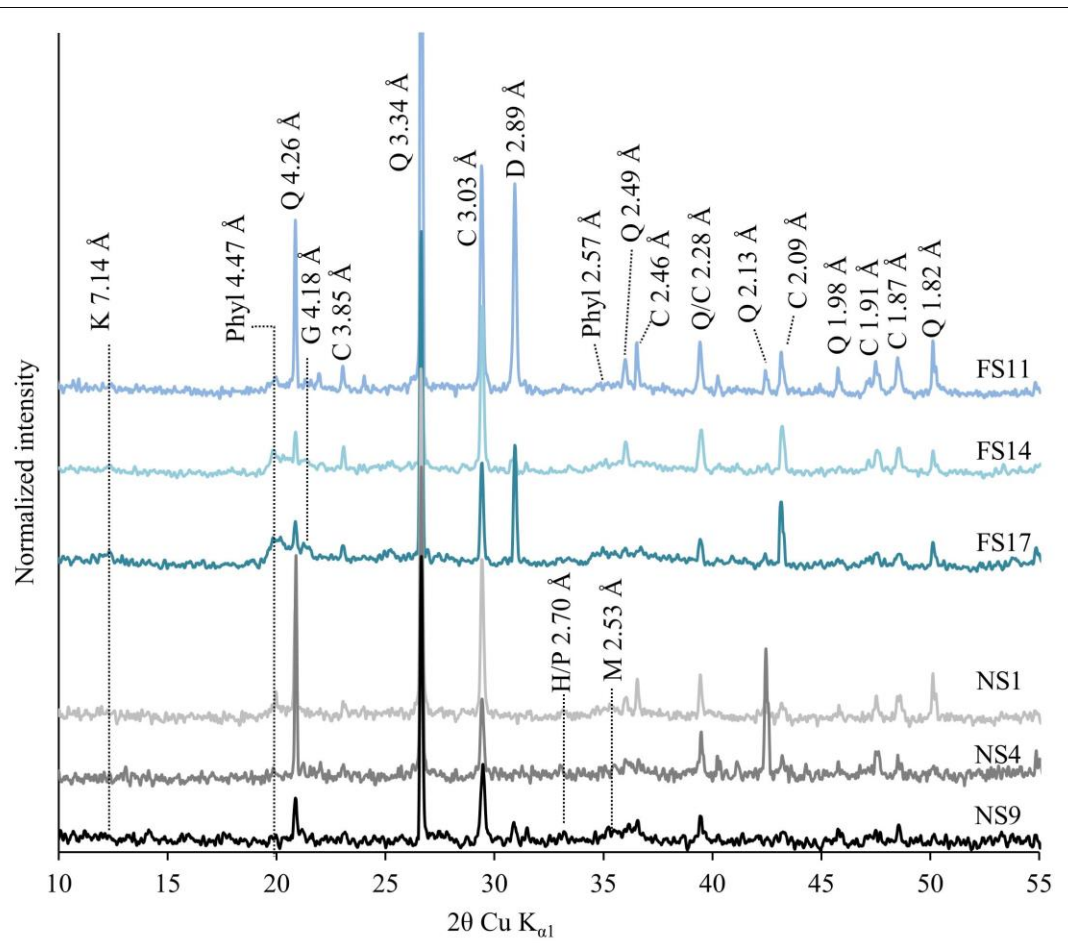


Fig. 4 XRD patterns for NS and FS technosols.

K: kaolinite, Phyl: phyllosilicates, Q: quartz, G: goethite, C: calcite, D: dolomite, H/P: hematite/pyrite, and M: magnetite

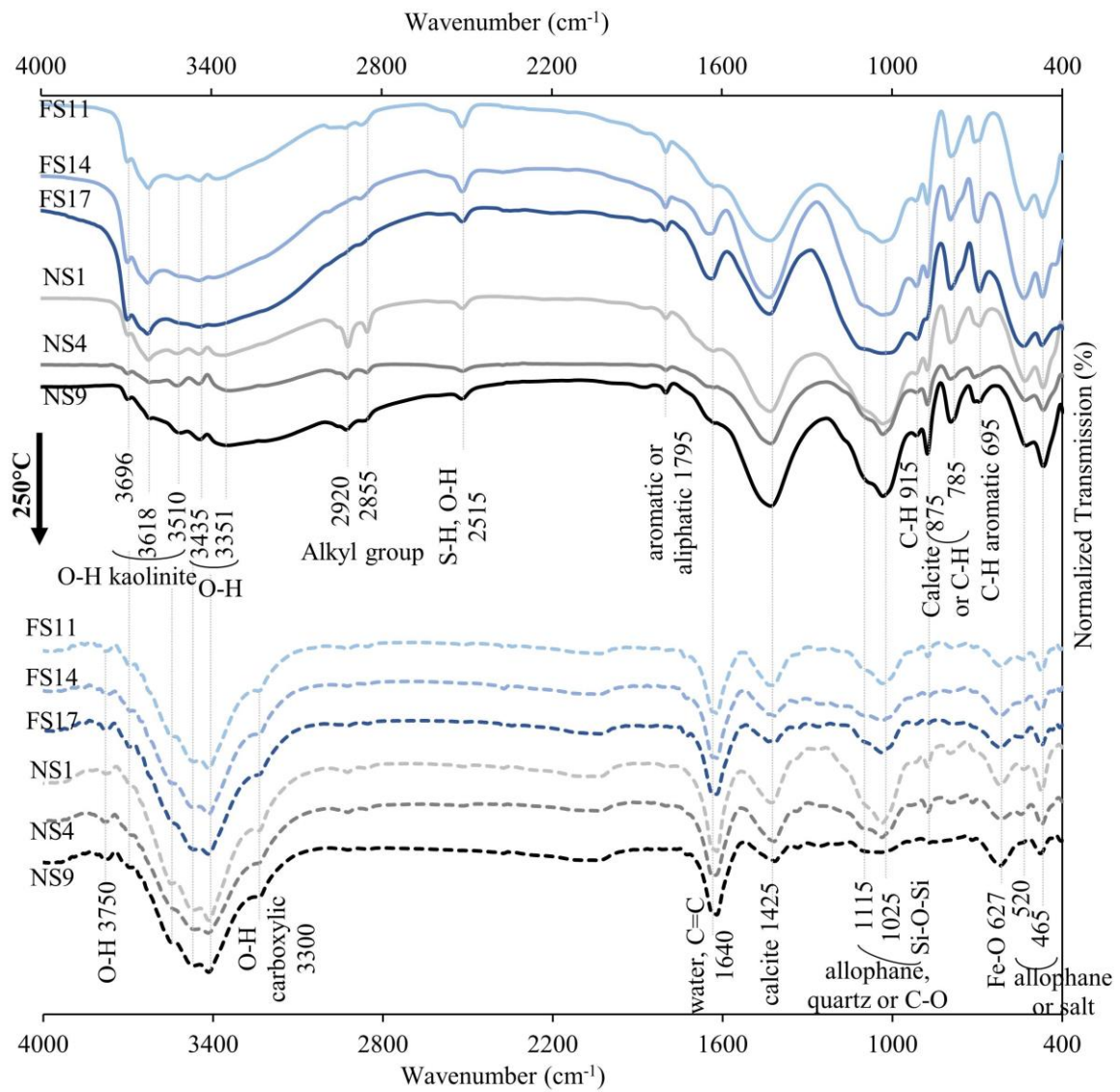


Fig. 5 FTIR spectra for selected NS and FS technosol layers before (top) and after calcination (bottom)

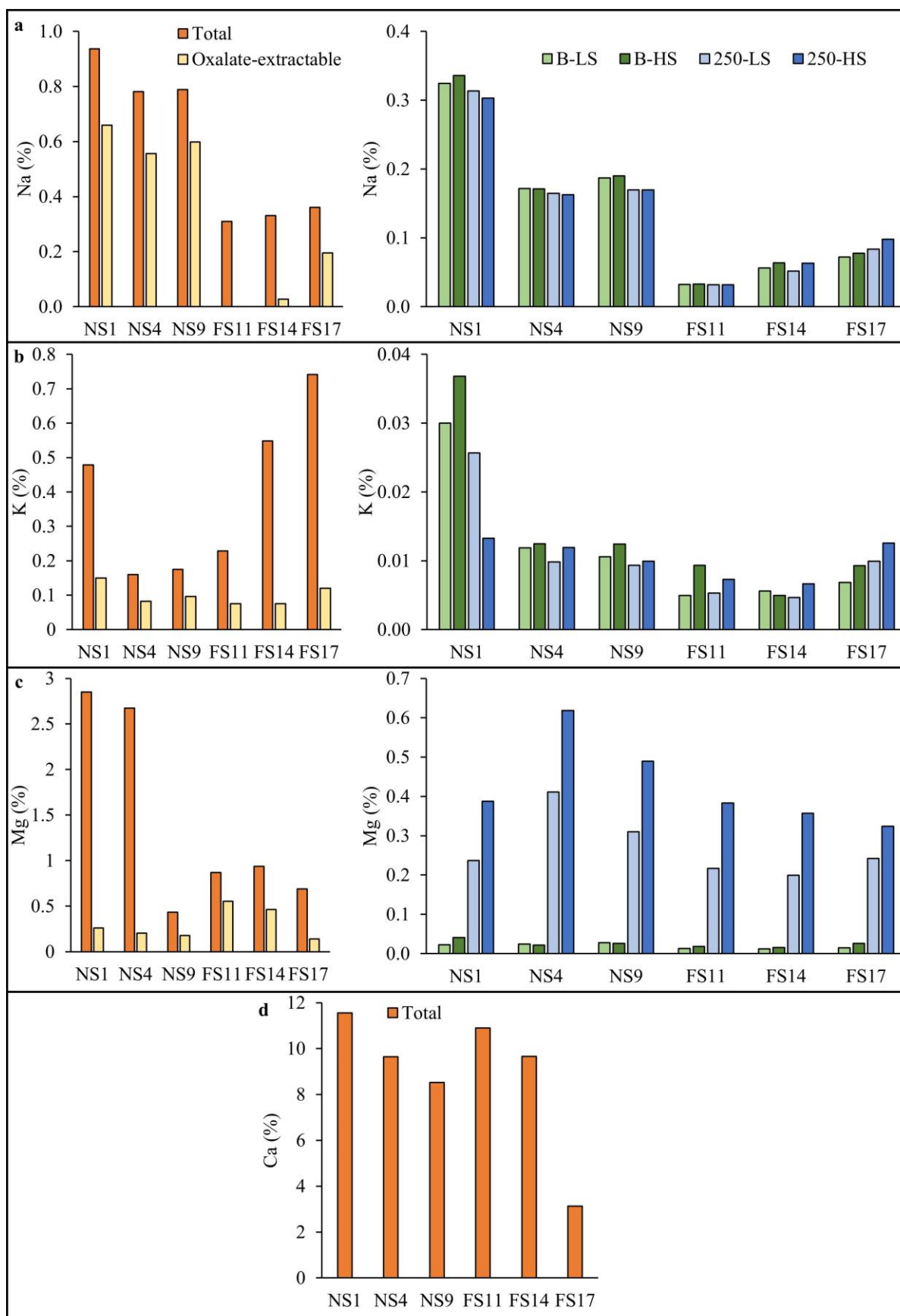


Fig. 6 Total and oxalate-extractable metal contents (Na, K, Mg and Ca), and extractable metals after desorption experiments for bulk (termed B) and calcinated samples (termed 250) using high and low salt concentrations (LS and HS, respectively)

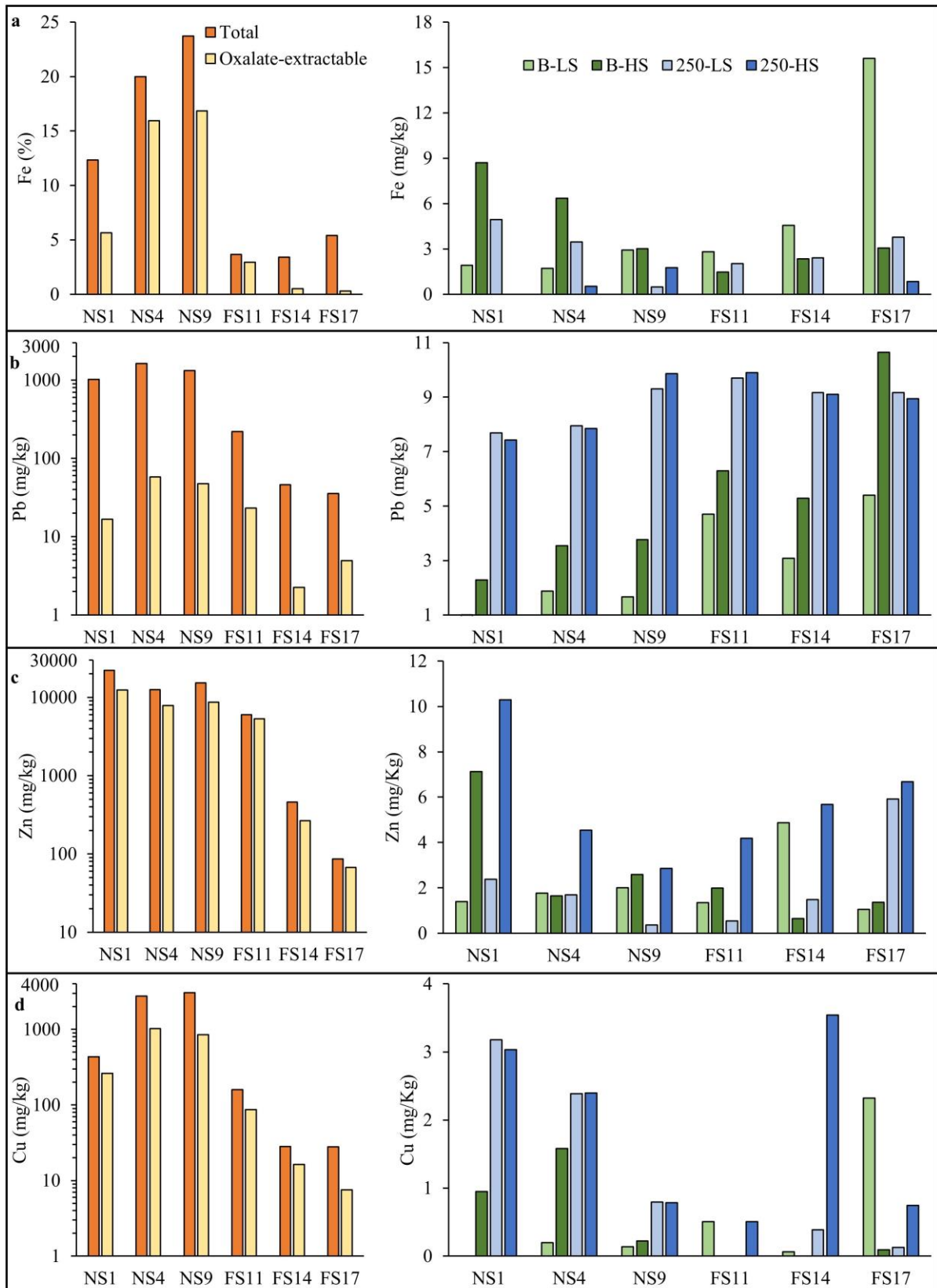


Fig. 7 Total and oxalate-extractable metal contents (Fe, Pb, Zn and Cu), and extractable metals after desorption experiments for bulk (termed B) and calcinated samples (termed 250) using high and low salt concentrations (LS and HS, respectively)

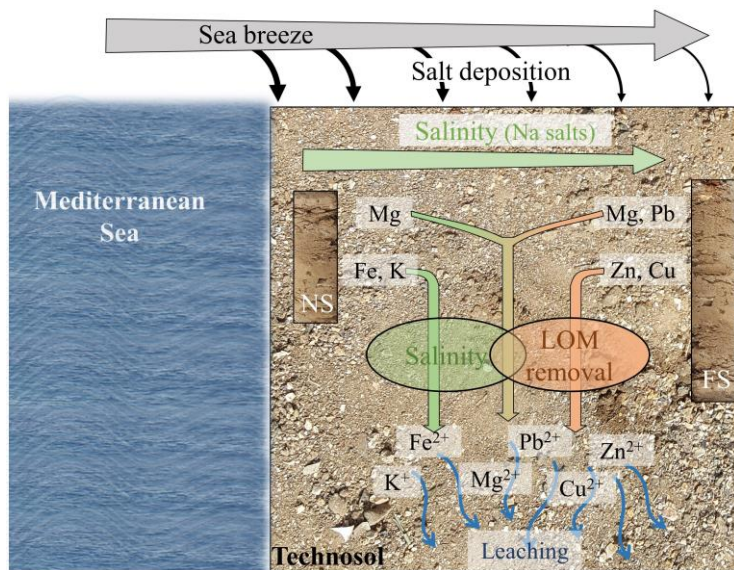


Fig. 8 Schematic representation of the fate of metals upon contact with saline solutions and removal of labile organic matter. The salinity of the technosols decreases when the location becomes farther from the sea due to salt deposition reduction. Salinity was shown to promote K and Fe release from the NS technosol layers; LOM removal was shown to promote Zn and Cu release from FS technosol layers; the combined effect of salinity and LOM removal was shown to promote Mg release in NS and FS technosol layers and Pb release in the FS technosol layers. The released metals indicated by cations are capable of leaching to water bodies (sea or groundwater).

7. Online Resource

Table A1: pH, salinity, EC, TDS, LOM, OM, D₁₀, D₅₀ and D₉₀ values for NS and FS samples. The same values were used to plot Fig. 2.

Samples	Depth cm	pH	Salinity (mg/L)	EC (µS/cm)	TDS (mg/L)	LOM (%)	OM (%)	D ₁₀ (µm)	D ₅₀ (µm)	D ₉₀ (µm)
NS1	0-3	7.9	1330	2719	1860	4.8	13.3	6.0	43	956
NS2	3-6	8.0	1160	2129	1630	4.3	11.2	6.3	132	114
NS3	6-10	7.9	1040	1969	1460	-	-	6.2	51	410
NS4	10-20	7.8	1240	2359	1660	5.3	11.5	11.6	344	1350
NS5	20-22	7.8	1120	2169	1580	-	-	7.3	132	717
NS6	22-26	7.9	1130	2009	1570	4.9	11.5	7.8	107	847
NS7	26-30	7.8	1620	3149	2280	4.8	12.1	6.9	268	2197
NS8	30-35	7.7	1920	3509	2680	-	-	6.1	45	622
NS9	35-40	7.8	1190	2149	1680	5.5	12.5	9.6	184	908
FS 10	0-4	8.1	210	456	300	3.3	9.9	5.4	19	321
FS 11	4-8	8.1	220	441	310	2.5	7.7	5.6	27	709
FS 14	19-24	8.1	190	374	260	4.1	10.8	0.2	6	90
FS 15	24-32	7.9	320	615	440	4.7	12.1	0.3	8	98
FS 17	50-55	7.6	230	453	330	4.9	12.6	2.3	10	64
FS 23	81-87	7.8	200	403	280	5.9	14.6	0.1	3	32

Table A2: Correlation of total metal contents, oxalate-extractable (OE) metal contents, and metal contents released from bulk (B) and calcinated (250) samples after desorption using low (LS) and high salinity (HS) solutions.

659

Na	OE	B-LS	B-HS	250-LS	250-HS
Total	.980	.951	.941	.936	.927
OE		.914	.902	.904	.902
B-LS			.999	.997	.993
B-HS				.998	.995
250-LS					.998

Fe	OE	B-LS	B-HS	250-LS	250-HS
Total	.970	-.426	.418	-.259	.690
OE		-.525	.311	-.354	.625
B-LS			-.322	.198	.198
B-HS				.720	-.180
250-LS					-.566

K	OE	B-LS	B-HS	250-LS	250-HS
Total	.470	.022	.028	.162	.205
OE		.809	.834	.907	.787
B-LS			.985	.979	.655
B-HS				.981	.638
250-LS					.747

Pb	OE	B-LS	B-HS	250-LS	250-HS
Total	.891	-.749	-.730	-.620	-.418
OE		-.413	-.523	-.270	-.065
B-LS			.919	.744	.588
B-HS				.574	.397
250-LS					.969

Mg	OE	B-LS	B-HS	250-LS	250-HS
Total	-.176	.372	.543	.414	.441
OE		-.667	-.516	-.566	-.332
B-LS			.496	.743	.732
B-HS				.017	-.068
250-LS					.950

Cu	OE	B-LS	B-HS	250-LS	250-HS
Total	.976	-.370	.513	.316	-.142
OE		-.413	.683	.469	-.032
B-LS			-.334	-.474	-.531
B-HS				.867	.395
250-LS					.556

Zn	OE	B-LS	B-HS	250-LS	250-HS
Total	.987	-.372	.837	-.368	.298
OE		-.423	.809	-.434	.238
B-LS			-.401	-.311	-.139
B-HS				-.036	.717
250-LS					.486